

# Asymmetric Coupled CMOS Lines—An Experimental Study

Uwe Arz, *Student Member, IEEE*, Dylan F. Williams, *Senior Member, IEEE*, David K. Walker, and Hartmut Grabinski

**Abstract**—This paper investigates the properties of asymmetric coupled lines built in a 0.25- $\mu\text{m}$  CMOS technology over the frequency range of 50 MHz to 26.5 GHz. We show that the frequency-dependent line parameters extracted from calibrated four-port scattering-parameter measurements agree well with numerical predictions. We also demonstrate by measurement and calculation that the two fundamental modes of the coupled-line system share significant cross power. To our knowledge, this is the first complete experimental characterization of asymmetric coupled lines on silicon ever reported.

**Index Terms**—Coupled mode analysis, integrated circuit interconnections, measurement, multiconductor transmission line, parameter estimation, silicon.

## I. INTRODUCTION

TRANSMISSION lines on semiconducting substrates have been investigated for many years. In 1971, Hasegawa *et al.* presented an analysis of microstrip lines on an Si-SiO<sub>2</sub> system [1]. Since this classic paper, numerous papers have been published, mostly dedicated to quasi-TEM analyses and the development of simple equivalent-circuit models.

Most of the publications dealing with the experimental characterization of these transmission lines have been restricted to the single-mode transmission-line case [2]–[5]. References [6] and [7] report on scattering-parameter-based coupled-line measurements on *conductive* substrates. However, [6] and [7] assume that the relationship between modal and conductor quantities is fixed and frequency independent. As a result, the measurement methods described in these references are applicable only to symmetrical coupled-line systems. References [8] and [9] investigate asymmetric coupled lines on *insulating* substrates.

In this paper, we study asymmetric coupled lines built on a conductive substrate. We extend the study reported in [10], examining not only the matrices of transmission-line parameters, but also the effects of substrate conductivity, the relationship between modal and conductor representations, and the modal cross powers.

The high conductivity of the CMOS substrate leads to a complex frequency-dependent behavior. The conductors are built in the second metallization layer of a six-metal-layer 0.25- $\mu\text{m}$

CMOS technology. The vias connecting the probe contact pads on the top metal layer (metal 6) with the second metal layer (metal 2), where the coupled-line systems are built, may affect the measurements. The access lines that connect the via stack below the contact pads with the coupled-line segment in the second metal level are subject to the same substrate effects as the coupled-line segment, and must also be accounted for.

In our approach, which is based on the method presented in [8], we express the electrical characteristics of the coupled-line system in terms of the frequency-dependent transmission-line parameters. The analysis uses the electrical model for multiconductor transmission lines and the nonlinear-regression method presented in [8]. However, [8] utilized a series of two-port measurements to characterize the coupled lines. Here, we investigate the more general problem of asymmetric coupled lines on a conductive substrate with the aid of fully calibrated four-port scattering-parameter measurements of the coupled lines, using the state-of-the-art on-wafer measurement and deembedding techniques described in [5], [11], and [12]. We pay special attention to the parasitic effects in the test structures (contact pads, vias between different metallization layers, and access lines).

Wherever possible, we use the quasi-analytical method of [13] to verify the experimental data. This procedure calculates the frequency-dependent line parameters of multiconductor transmission-line systems on conductive substrates from their cross-sectional data. This is based on the assumption that the skin effect in the conductive substrate affects only the calculation of the impedance parameters. Furthermore, the skin effect in the signal and ground conductors is neglected. We also use the quasi-analytical calculations of [13] to demonstrate the influence of the substrate conductivity on the transmission-line parameters.

In Section VI, we investigate the modal behavior of the asymmetric coupled lines by determining the ratio of conductor voltages for  $c$ - and  $\pi$ -mode excitation, and by calculating the cross power shared between the two fundamental modes from measured and predicted line-parameter values.

## II. EXPERIMENTAL SETUP

The cross section of the lines we studied is shown in Fig. 1(a), and the top view of the coupled-line system is shown in Fig. 1(b). The coupled conductors are fabricated in the second level of metal, which has a thickness of 0.7  $\mu\text{m}$  and a metal conductivity of  $27.8 \times 10^6$  S/m. The first conductor has a width of 1  $\mu\text{m}$ , the second a width of 10  $\mu\text{m}$ , and the two coupled conductors are separated by a gap of 1  $\mu\text{m}$ . The conductivity of the silicon substrate is  $10^4$  S/m. Two 20- $\mu\text{m}$ -wide

Manuscript received March 6, 2000. This work was supported in part under an Automatic RF Techniques Group Student Fellowship.

U. Arz and H. Grabinski are with the Laboratory of Information Technology, University of Hannover, 30167 Hannover, Germany (e-mail: uwe@lfi.uni-hannover.de).

D. F. Williams and D. K. Walker are with the National Institute of Standards and Technology, Boulder, CO 80303 USA.

Publisher Item Identifier S 0018-9480(00)10767-7.

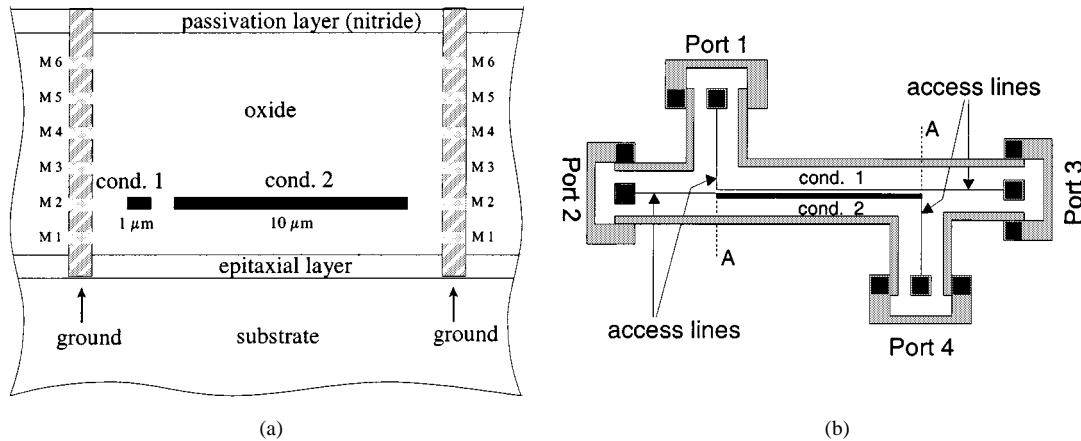


Fig. 1. Test structures. (a) Cross section. (b) Top view.

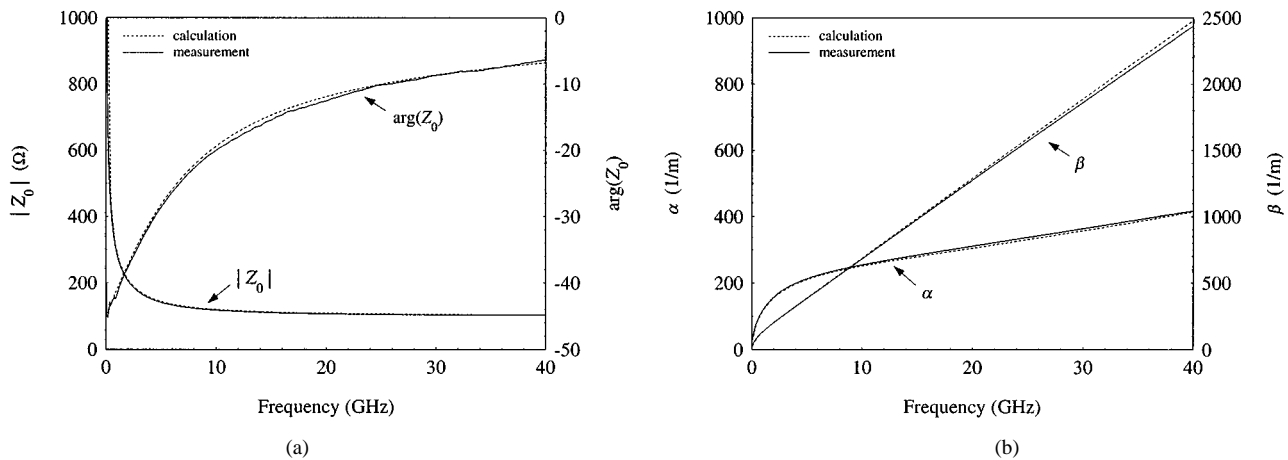


Fig. 2. Characteristic impedance  $Z_0$  and propagation constant  $\gamma = \alpha + j\beta$  of the 1- $\mu\text{m}$ -wide access lines in metal 2. (a) Magnitude and phase of characteristic impedance  $Z_0$ . (b) Real ( $\alpha$ ) and imaginary ( $\beta$ ) parts of the propagation constant ( $\gamma$ ).

grounds composed of via stacks connecting the substrate and all six metallization layers together are located on each side of the coupled lines. The distance between the grounds and the center of the coupled-line structure is 65  $\mu\text{m}$ .

We used on-wafer probes to connect to the four 50  $\mu\text{m} \times 50 \mu\text{m}$  contact pads on the top metal layer. Via stacks connect the contact pads to the access lines of the coupled-line system, which were fabricated in the second metal level. The width of the access lines is 1  $\mu\text{m}$ , and their length is 200  $\mu\text{m}$ . The lengths of the coupled-line segments are 0.5, 1.0, and 2.5 mm.

We also fabricated test structures to characterize the single-mode access lines. These 1- $\mu\text{m}$ -wide lines were built in the second metal level and had lengths of 0.5, 1.0, and 2.5 mm.

### III. MEASUREMENT AND DEEMBEDDING PROCEDURE

We used two-port measurements to characterize the contacts and access lines. We first performed a 50- $\Omega$  multilayer thru-reflect-line (TRL) reference calibration [11] in coplanar lines fabricated on a semiinsulating gallium-arsenide substrate, and moved the calibration reference plane back to the probe tips. We then performed a second-tier TRL calibration in the access lines on the silicon substrate, in which we had fabricated the

coupled lines. Here, we employed the “calibration comparison” method [5], which is designed to be insensitive to large contact-pad capacitance, to determine the characteristic impedance  $Z_0$  of the access lines. We then used this information to reset the reference impedance of the second-tier TRL calibration to 50  $\Omega$ . This procedure determined an “error box” describing the electrical behavior of the contact pads, vias, and access lines.

Fig. 2 shows the characteristic impedance  $Z_0$  and the propagation constant  $\gamma$  of the 1- $\mu\text{m}$ -wide access lines fabricated in the second-level metal. The solid lines indicate measurement results obtained using the method of [5], and the dashed lines correspond to calculations obtained using the quasi-analytical procedure of [13]. The negative phase of  $Z_0$  indicates that the longitudinal losses are dominant.

The agreement is excellent over the entire frequency range of 0.2–40 GHz. The maximum deviations observed between the measured and calculated values of Fig. 2 correspond to relative errors of less than 2.5%. Considering the difficulties typical of on-chip probing on silicon these results rank among the most accurate ever reported.

The calibration procedure used for the four-port measurement is described in [12]. It eliminates the need for orthogonal calibration standards, and requires only three in-line calibrations. To this end, we again used the multilayer TRL procedure [11].

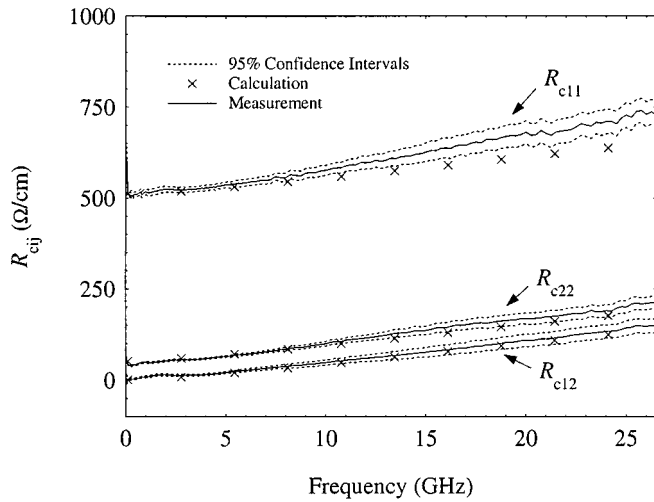


Fig. 3. Resistances per unit length.

Since the initial reference-plane position of the four-port calibration was “at the probe tips,” we used an additional deembedding step for the access lines. We employed the error boxes determined by the second-tier TRL calibration in the access lines for this purpose, using the propagation constant from the TRL calibration to set the reference planes to the beginning of the coupled-line segment (marked *A* in Fig. 1).

#### IV. COUPLED-LINE ANALYSIS

The coupled lines we study support two dominant modes, which are commonly called the *c* and  $\pi$  modes, and which correspond to the even and odd modes in the symmetric case. The relationship between modal (subscript *m*) and conductor representations (subscript *c*) of the voltage and current vectors in a multiconductor transmission line is given by [14]

$$\mathbf{v}_c = \mathbf{M}_v \mathbf{v}_m \quad \text{and} \quad \mathbf{i}_c = \mathbf{M}_i \mathbf{i}_m. \quad (1)$$

These vectors satisfy the transmission-line equations

$$d\mathbf{v}_c/dz = -\mathbf{Z}_c \mathbf{i}_c \quad \text{and} \quad d\mathbf{i}_c/dz = -\mathbf{Y}_c \mathbf{v}_c \quad (2)$$

where the matrices of conductor impedances and admittances per unit length are defined by  $\mathbf{Z}_c \equiv \mathbf{R}_c + j\omega\mathbf{L}_c$  and  $\mathbf{Y}_c \equiv \mathbf{G}_c + j\omega\mathbf{C}_c$ .

We chose the voltage paths between each of the two conductors and the ground. We then used the method of [8] to determine  $\mathbf{M}_v$ ,  $\mathbf{M}_i$ , and the matrices of the line parameters  $\mathbf{R}_c$ ,  $\mathbf{L}_c$ ,  $\mathbf{G}_c$ , and  $\mathbf{C}_c$  in the conductor representation of [14]. The vectors  $\mathbf{v}_c$  and  $\mathbf{i}_c$  are power normalized according to the theories presented in [14] and [15]. This is equivalent to the requirement that the total complex power *p* carried in the forward direction is

$$p = \mathbf{i}_m^\dagger \mathbf{X} \mathbf{v}_m = \mathbf{i}_c^\dagger \mathbf{v}_c \quad (3)$$

where the diagonal elements of the cross-power matrix  $\mathbf{X}$  are equal to one and  $^\dagger$  indicates the Hermitian adjoint (conjugate transpose).

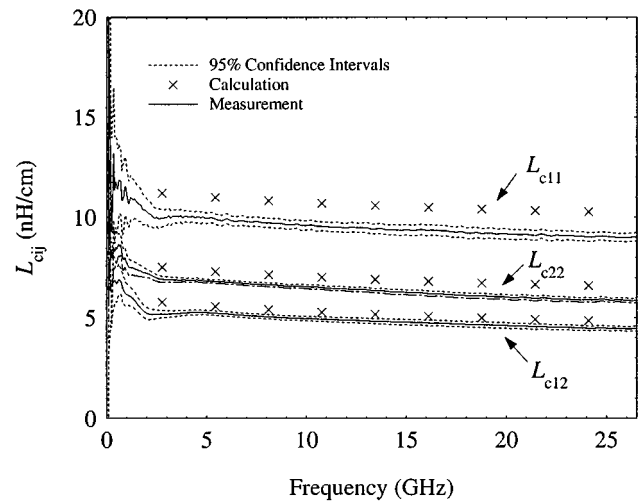
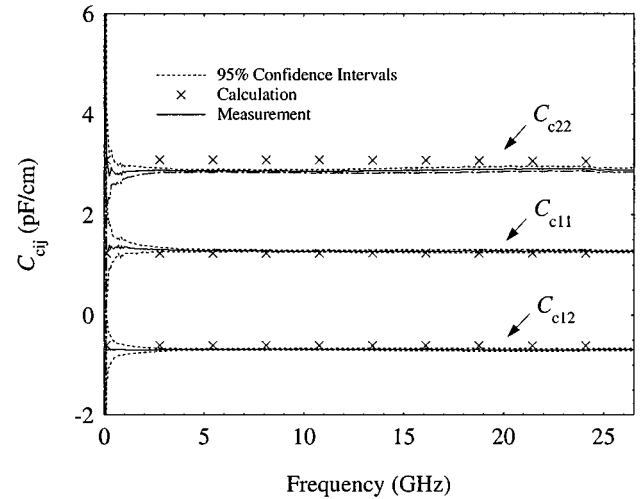


Fig. 4. Inductances per unit length.

Fig. 5. Capacitances per unit length.  $C_{c12}$  is negative due to the current definitions used to define the conductors parameters (see [14, Fig. 4]).

We estimated the line-parameter matrices from the four-port measurement data using the weighted orthogonal-distance regression algorithm of [16] and the procedure in [8]. This procedure solved for all of the elements of  $\mathbf{R}_c$ ,  $\mathbf{L}_c$ ,  $\mathbf{G}_c$ , and  $\mathbf{C}_c$  at each frequency point independently.

Using the method of [13], we calculated the starting values for the lowest frequency. We then used the results of the optimization at each frequency point as starting values for the optimization at the next higher frequency point. Additional investigations showed that the optimization algorithm converged to virtually identical results even when the dc values were chosen as the starting values over the entire frequency range.

Reference [8] compares two methods of determining  $\mathbf{R}_c$ ,  $\mathbf{L}_c$ ,  $\mathbf{G}_c$ , and  $\mathbf{C}_c$ . The first method, which we employed here, determines  $\mathbf{R}_c$ ,  $\mathbf{L}_c$ ,  $\mathbf{G}_c$ , and  $\mathbf{C}_c$  directly, but ignores the four-port error boxes describing the discontinuities where the access lines connect to the coupled lines. The second method studied in [8] requires that the capacitance be flat and  $\mathbf{G}_c$  be small, but accounts for the four-port error boxes.

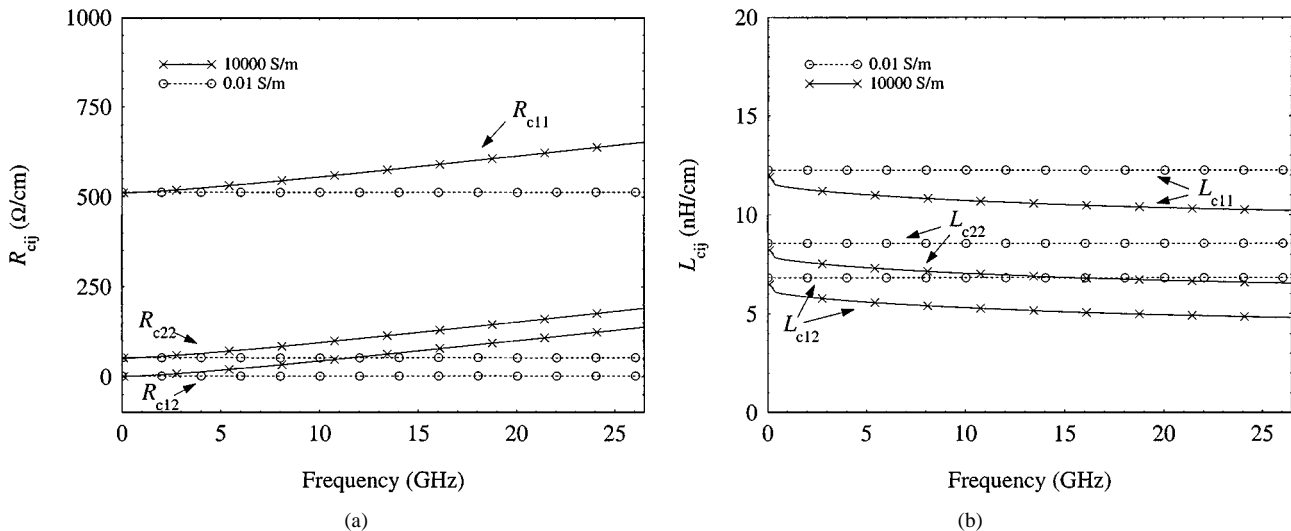


Fig. 6. Influence of substrate resistivity ( $\sigma = 10\,000 \text{ S/m}$  versus  $\sigma = 0.01 \text{ S/m}$ ). (a) Resistance per unit length of coupled-line system. (b) Inductances per unit length of coupled-line system.

In our analysis, we ignored the four-port error boxes that represent the discontinuities between the single-mode access lines and the multimode coupled-line segment. We felt that this was justified by the small sizes of those discontinuities. Although we did not implement the second method of [8], which does account for these discontinuities, the measurements we reported here indicate that  $\mathbf{C}_c$  is flat enough and  $\mathbf{G}_c$  small enough to allow its use.

We also used the regression method of [16] to characterize the random error in the redundant four-port measurement data. The analysis determines 95% confidence intervals for the estimated results over the entire frequency range under the assumption that the error sources in the experiment are entirely random, independent, and normally distributed. Figs. 3–5 show the estimated line parameters of the asymmetric coupled-line system (labeled “measurement”), the lower and upper bounds for the 95% confidence intervals, and the line parameters calculated from the quasi-analytical formulas given in [13] (labeled “calculation”).

The values estimated for the elements  $\mathbf{G}_c$ , which are not presented here, are all smaller than  $0.02 \text{ S/cm}$  over the whole frequency range and do not have a significant effect on the signal propagation behavior of the coupled-line system. We verified this assertion by fixing all elements of  $\mathbf{G}_c$  to zero during the nonlinear optimization process. The results for  $\mathbf{C}_c$  and  $\mathbf{L}_c$  were virtually indistinguishable, and the elements of  $\mathbf{R}_c$  deteriorated only slightly when compared to the calculations of [13].

The agreement between measured and calculated values is good over the entire frequency band. However, some of the calculated values fall outside of the 95% confidence intervals for the estimated parameters. This is a clear indication that there is still some systematic error in either the measurements or the calculations. Sources of systematic error in the measurements include our neglect of the four-port error boxes describing the transition between access lines and coupled-line segment. Errors in the calculation using the method of [13] can probably be traced back to uncertainties in the information from the manufacturer about the cross-sectional parameters of the six-layer CMOS process.

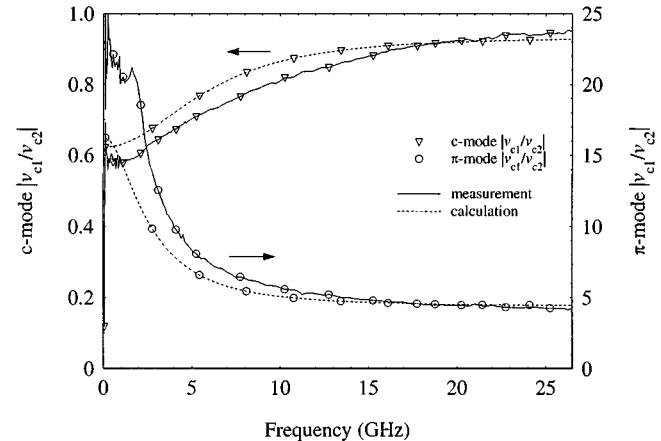


Fig. 7. Ratio of conductor voltages of the  $c$  and  $\pi$  modes. Arrows indicate the appropriate scales.

## V. SUBSTRATE EFFECTS

Hasegawa *et al.* [1] identify three typical regions of operation<sup>1</sup> in their paper on the analysis of microstrip lines in Si–SiO<sub>2</sub> systems: the “slow-wave” region, the “skin-effect” region, and the “dielectric quasi-TEM” region. However, this classification is introduced for the case of a single-mode transmission-line system only. It is the purpose of this section to investigate whether similar phenomena can be observed in coupled CMOS transmission lines as well.

From the results reported in [8], we know that the resistances and inductances per unit length only show a weak dependence on the frequency for insulating substrates. We also tried to examine this aspect for the CMOS coupled-line system by calculating the line parameters for the test structures of Fig. 1, but assuming that the substrate conductivity is very low. The comparison to the actual values is shown in Fig. 6.

<sup>1</sup>In [1], Hasegawa *et al.* are speaking of “modes” of operation. In order to avoid confusion with the  $c$  and  $\pi$  modes discussed in Section IV, we prefer to speak of “regions” of operation, which we believe to be a more appropriate term.

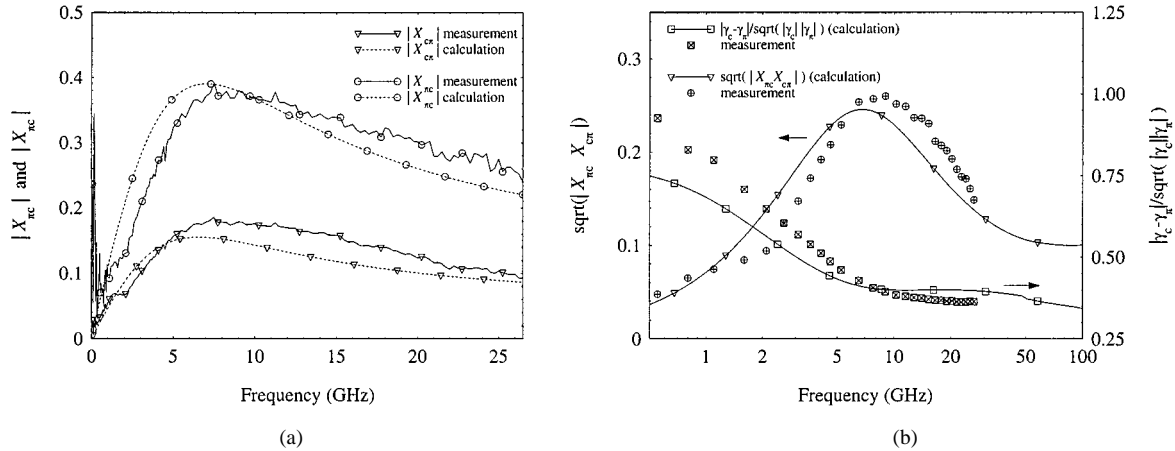


Fig. 8. Magnitude of modal cross power. Arrows indicate the appropriate scales for the plotted data. (a) Magnitude of  $X_{\pi c}$  and  $X_{c\pi}$ . (b) Magnitude of  $\sqrt{|X_{\pi c} X_{c\pi}|}$  and  $\frac{|\gamma_c - \gamma_\pi|}{\sqrt{|\gamma_c \gamma_\pi|}}$ .

The resistances and inductances per unit length on an insulating substrate stay nearly constant with frequency. However, the resistance and inductance of our structures is clearly frequency dependent. This leads to the conclusion that the measured frequency dependence must be attributed to the skin effect in the substrate. This is also confirmed by the fact that the skin depth at our highest measurement frequency of 26.5 GHz is  $0.59 \mu\text{m}$  in the conductor metal and  $30.9 \mu\text{m}$  in the substrate. Thus, the skin effect in the conductor metal plays only a minor role and can be neglected.

## VI. MODAL CROSS POWER

Fig. 7 shows the ratios of conductor voltage magnitudes  $|v_{c1}/v_{c2}|$  for the  $c$  and  $\pi$  mode determined from our measurements and calculations, which we determined from (1) using

$$\frac{v_{c1}}{v_{c2}} = \frac{M_{v11}}{M_{v21}} \text{ (} c\text{-mode)} \quad \text{and} \quad \frac{v_{c1}}{v_{c2}} = \frac{M_{v12}}{M_{v22}} \text{ (} \pi\text{-mode)}. \quad (4)$$

Fig. 7 shows that these ratios are strongly frequency dependent, and confirms that the elements of  $\mathbf{M}_v$ , which describe the relationship between modal and conductor voltages, cannot be treated as fixed values. This clearly shows that the assumptions of the methods in [6] and [7] would fail in the case of asymmetric lines.

Fig. 8(a) and (b) compares measurements of the off-diagonal elements of the modal cross-power matrix  $\mathbf{X}$  [see (3)] to calculations based on the line parameters determined by the quasi-analytical method of [13]. Measurement and calculation are in fair agreement.

Fig. 8(a) shows that the cross power shared between the  $c$  and  $\pi$  modes of the asymmetric coupled-line system cannot be neglected, even at moderate frequencies. The physical reasons for this behavior have been investigated in [17] for the case of a nonconductive substrate. Despite the fact that the line parameters of the coupled-line structures investigated here have a much stronger frequency dependence than in [17], we also observe a significant rise in the cross power at intermediate frequencies.

We also tried to identify the frequency region where the cross power rises by examining the frequency-dependent propagation constants  $\gamma_c$  and  $\gamma_\pi$ . References [17] and [18] predict a rise in the cross power at frequencies where  $\gamma_c$  and  $\gamma_\pi$  are close. The corresponding curve of  $|\gamma_c - \gamma_\pi|/\sqrt{|\gamma_c \gamma_\pi|}$  in Fig. 8(b) shows that the difference between the propagation constants decreases with frequency. This indicates that the physical mechanisms leading to increased cross-power levels on lossy conductive substrates might be different from the ones observed in low-loss waveguides, where the cross powers rise over narrow frequency bands when the propagation constants of different modes become extremely close.

While the experimental data were available only up to 26.5 GHz, we were able to carry out the calculations of the line parameters with the method of [13] to 100 GHz. One obvious difference between the results reported here and in [17] is that the modal cross powers for the asymmetric structures investigated here do not vanish for the limiting case of very high frequencies, as can be seen from Fig. 8(b). Further investigations will be necessary to clarify the behavior predicted by [13] at the highest frequencies.

## VII. CONCLUSION

In this paper, we have investigated the properties of asymmetric coupled transmission lines built in a six-metal-level CMOS process. The on-wafer measurements presented here agree closely with quasi-analytical calculations over a broad-band frequency range. Measurement and calculations show that the skin effect in the highly conductive silicon substrate leads to a strong frequency dependence of the line parameters  $\mathbf{R}_c$  and  $\mathbf{L}_c$ . This effect was further investigated by comparing to calculations with a low-conductivity substrate.

We also have demonstrated by measurement and calculation that the relationship between modal and conductor quantities is frequency dependent, and that the two dominant modes share significant levels of cross power at moderate frequencies. This investigation shows that, for the important and practical case of CMOS transmission lines, power-normalized equivalent-circuit

theories, such as those outlined in [14] and [15], are required for an adequate treatment of these common circuit elements.

#### ACKNOWLEDGMENT

The authors would like to thank M. Rudack, Laboratory of Information Technology, Hannover University, Hannover, Germany, and D. Treytnar, Laboratory of Information Technology, Hannover University, Hannover, Germany, for their support with the layout and fabrication of the test structures. The authors also gratefully acknowledge the assistance of J. Rogers, formerly of the National Institute of Standards and Technology, Boulder, CO, in implementing the software in Fortran 90.

#### REFERENCES

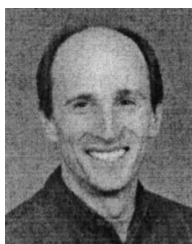
- [1] H. Hasegawa, M. Furukawa, and H. Janai, "Properties of microstrip line on Si-SiO<sub>2</sub> system," *IEEE Trans. Microwave Theory Tech.*, vol. MTT-15, pp. 869–881, Nov. 1971.
- [2] Y. Eo and W. R. Eisenstadt, "High-speed VLSI interconnect modeling based on *S*-parameter measurements," *IEEE Trans. Comp., Hybrids, Manufact. Technol.*, vol. 16, pp. 555–562, Aug. 1993.
- [3] S. Zaage and E. Grotelüschen, "Characterization of the broadband transmission behavior of interconnections on silicon substrates," *IEEE Trans. Comp., Hybrids, Manufact. Technol.*, vol. 16, pp. 686–691, Nov. 1993.
- [4] T.-M. Winkel, L. S. Dutta, and H. Grabinski, "An accurate determination of the characteristic impedance of lossy lines on chips based on high frequency *S*-parameter measurements," in *IEEE Multichip Module Conf. Dig.*, Feb. 1996, pp. 190–195.
- [5] D. F. Williams, U. Arz, and H. Grabinski, "Accurate characteristic impedance measurement on silicon," in *IEEE MTT-S Int. Microwave Symp. Dig.*, June 9–11, 1998, pp. 1917–1920.
- [6] T.-M. Winkel, L. S. Dutta, H. Grabinski, and E. Grotelüschen, "Determination of the propagation constant of coupled lines on chips based on high frequency measurements," in *IEEE Multichip Module Conf. Dig.*, Feb. 6–7, 1996, pp. 99–104.
- [7] T.-M. Winkel, L. S. Dutta, and H. Grabinski, "An accurate determination of the characteristic impedance matrix of symmetrical coupled lines on chips based on high frequency *S*-parameter measurements," in *IEEE MTT-S Int. Microwave Symp. Dig.*, June 8–13, 1997, pp. 1769–1772.
- [8] D. F. Williams, J. E. Rogers, and C. L. Holloway, "Multiconductor transmission line characterization: Representations, approximations, and accuracy," *IEEE Trans. Microwave Theory Tech.*, vol. 47, pp. 403–409, Apr. 1999.
- [9] C. Seguinot, P. Kennis, J.-F. Legier, F. Huret, E. Paleczny, and L. Hayden, "Multimode TRL—A new concept in microwave measurements: Theory and experimental verification," *IEEE Trans. Microwave Theory Tech.*, vol. 46, pp. 403–409, May 1998.
- [10] U. Arz, D. F. Williams, D. K. Walker, J. E. Rogers, M. Rudack, D. Treytnar, and H. Grabinski, "Characterization of asymmetric coupled CMOS lines," in *IEEE MTT-S Int. Microwave Symp. Dig.*, June 11–16, 2000, pp. 609–612.
- [11] R. B. Marks, "A multilayer method of network analyzer calibration," *IEEE Trans. Microwave Theory Tech.*, vol. 39, pp. 1205–1215, July 1991.
- [12] D. F. Williams and D. K. Walker, "In-line multiport calibration," in *51st ARFTG Conf. Dig.*, June 12, 1998, pp. 88–90.
- [13] E. Grotelüschen, L. S. Dutta, and S. Zaage, "Quasi-analytical analysis of the broad-band properties of multiconductor transmission lines on semiconducting substrates," *IEEE Trans. Comp., Packag., Manufact. Technol. B*, vol. 17, pp. 376–382, Aug. 1994.
- [14] D. F. Williams, L. A. Hayden, and R. B. Marks, "A complete multimode equivalent-circuit theory for electrical design," *J. Res. Natl. Bur. Stand.*, vol. 102, no. 4, pp. 405–423, July-Aug. 1997.
- [15] R. B. Marks and D. F. Williams, "A general waveguide circuit theory," *J. Res. Natl. Bur. Stand.*, vol. 97, no. 5, pp. 533–562, Sept.-Oct. 1992.
- [16] P. T. Boggs, R. H. Byrd, and R. D. Schnabel, "A stable and efficient algorithm for nonlinear orthogonal distance regression," *SIAM J. Sci. Stat. Comput.*, pp. 1052–1078, Nov. 1987.
- [17] D. F. Williams and F. Olyslager, "Modal cross-power in quasi-TEM transmission lines," *IEEE Microwave Guided Wave Lett.*, vol. 6, pp. 413–415, Nov. 1996.
- [18] D. F. Williams, "Thermal noise in lossy waveguides," *IEEE Trans. Microwave Theory Tech.*, vol. 44, pp. 1067–1073, July 1996.



**Uwe Arz** (S'97) received the Dipl.-Ing. degree from the University of Hannover, Hannover, Germany, in 1994, and is currently working toward the Ph.D. degree in the area of on-chip interconnect measurement methods at the University of Hannover.

Since 1995, he has been a Research and Teaching Assistant in the Laboratory of Information Technology, University of Hannover. His research interests include broad-band characterization methods for high-speed digital interconnects and packages.

Mr. Arz was the recipient of the first ARFTG Microwave Measurement Fellowship Award.



**Dylan F. Williams** (S'82–M'86–SM'90) received the Ph.D. degree in electrical engineering from the University of California at Berkeley, in 1986.

In 1989, he joined the Electromagnetic Fields Division, National Institute of Standards and Technology, where he currently develops metrology for the characterization of monolithic microwave integrated circuits and electronic interconnects. He has authored or co-authored over 60 technical papers.

Dr. Williams was the recipient of the Department of Commerce Bronze and Silver Medals, the Electrical Engineering Laboratory's Outstanding Paper Award, two ARFTG Best Paper Awards, the ARFTG Automated Measurements Technology Award, and the IEEE Morris E. Leeds Award.

**David K. Walker** received the B.A. degree in physics and mathematics from Hastings College, Hastings, NE, and the B.S. and M.S. degrees in electrical engineering from Washington University, St. Louis, MO, in 1982 and 1983, respectively.

He spent eight years in industry, where he was involved with microwave semiconductor device design and fabrication before joining the National Institute of Standards and Technology (NIST), Boulder, CO, in 1991 as part of the monolithic-microwave integrated-circuit (MMIC) project of the Microwave Metrology Group. His work at NIST includes semiconductor fabrication and network analyzer calibration and measurement in the on-wafer environment. He holds five patents related to microwave technology.



**Hartmut Grabinski** was born in Hildesheim, Germany. He received the Dipl.-Ing. degree from Fachhochschule Hannover, Hannover, Germany, in 1977, the Dipl.-Ing. and Dr.-Ing. degrees from University of Hannover, Hannover, Germany, in 1982 and 1987, respectively, and the Dr.-Ing. habil. degree in Theoretische Elektrotechnik from the University of Hannover, in 1993.

He is currently a Lecturer in the Department of Electrical Engineering, University of Hannover. Since 1987, he has been the Manager of the Design & Test Division, Laboratory of Information Technology, University of Hannover. His research interests include electro-dynamics of interconnects and electrical performance of electronic packaging.